Nanoscale

COMMUNICATION

View Article Online
View Journal | View Issue

Cite this: *Nanoscale*, 2017, **9**, 7755

Received 21st April 2017,
Accepted 16th May 2017

DOI: 10.1039/c7nr02841e

rsc.li/nanoscale

CdS-coated TiO_2 nanotube layers: downscaling tube diameter towards efficient heterostructured photoelectrochemical conversion

M. Krbal, J. Prikryl, R. Zazpe, H. Sopha and J. M. Macak *

Herein, a novel photoelectrochemical heterostructure based on TiO_2 nanotube layers uniformly coated by a CdS thin layer (using ALD) is presented. Downscaling the nanotube diameter (from 95 to 35 nm) resulted in a 2-fold enhancement of the UV and Vis light photocurrents. Further photocurrent improvement resulted from the prior annealing of the TiO_2 nanotube layers from 300 to 600 °C.

The ever increasing demand for a long-term replacement of fossil fuels by low-cost, highly-efficient, renewable, and environmentally friendly sources of energy has led to significant development of photovoltaic technologies. Next to silicon[1,2] and chalcogenide[3–5] solar cells, recently, new types of thin film-based devices employing TiO_2 mesoporous structures sensitized with organic dyes,[6] perovskites,[7] and quantum dots[8–10] have been designed and developed. For these devices, the main challenge is to select an appropriate TiO_2 and chromophore couple. However, it was shown that *via* controlling the TiO_2–chromophore interface, the efficiency of the cells could be increased.[6,11] This enhancement can be achieved by increasing the interfacial surface area between the chromophore and TiO_2 to facilitate efficient charge separation. Unlike mesoporous TiO_2 supports, ordered nanostructures, such as high aspect ratio self-organized TiO_2 nanotube layers[12,13] or TiO_2 nanorods,[14,15] offer the advantage of directed charge transport and controlled phase separation between donor and acceptor parts of the solar cell; thus, they seem very promising for nanoscale solar hybrid technologies.[16,17]

In the case of 1D self-organized TiO_2 nanostructures, the overall surface can be easily increased by prolonging their length or reducing their diameters while increasing their number. Especially, self-organized TiO_2 nanotube layers possess inner and outer surfaces of tubes, which are highly beneficial as compared to nanowires[18] or nanorods.[14,15] To achieve higher power conversion efficiency levels, the surface can be, in a further step, coated by a secondary material using chemical bath deposition,[8,19] spincoating,[20,21] sputtering,[22] electrodeposition,[23] a solvothermal method,[24,25] and atomic layer deposition (ALD).[26–28] However, only the ALD technique leads to the homogeneous covering of the nanotube interiors as well as exteriors,[27,28] thus ensuring the best possible TiO_2–chromophore interface, especially for high-aspect ratio nanotubes.

Herein, we present photoelectrochemical and structural characterization of a new type of heterostructured photochemical half-cells; these cells were fabricated using highly ordered n-type conductive TiO_2 nanotubular scaffolds, with different diameters (35, 56, and 95 nm), coated by CdS (40 cycles, thickness ~6 nm) that was deposited *via* a tailored ALD process.

The TiO_2 nanotube layers used in our experiments were prepared by anodization of the Ti foils. The anodization conditions for these layers with similar thicknesses and different nanotube inner diameters have been previously described.[19] Prior to the deposition of CdS, amorphous nanotube layers were converted to anatase/rutile phases using the previously applied annealing protocol[29] in the temperature range from 300 to 600 °C.

In the second step, TiO_2 nanotube layers were coated for the first time by CdS *via* ALD (TFS200, Beneq) using the following conditions. Dimethylcadmium (electronic grade 99.999%) and gaseous H_2S were used as the cadmium precursor and the sulphur source, respectively. High purity nitrogen (99.9999%) was the carrier and purging gas at a flow rate of 400 standard cubic centimetres minute (sccm). Under these deposition conditions, one growth ALD cycle was defined by the following sequence: dimethylcadmium pulse (400 ms)-N_2 purge (10 s)-H_2S pulse (1 s)-N_2 purge (15 s). The TiO_2 nanotube layers were CdS-coated at 150 °C by applying 40 ALD cycles. This corresponds to a nominal thickness of approx. 6 nm, as confirmed by variable angle spectroscopic ellipsometry (VASE® ellipsometer, J.A. Woollam, Co., Inc.) of CdS coatings on Si wafers. The composition of CdS deposited *via* ALD on a Si wafer was verified using XPS, which showed the Cd : S ratio to be 1 : 1. The morphology of the TiO_2 nanotube layers was characterized by field-emission SEM (FE SEM JEOL JSM 7500F) and high

Center of Materials and Nanotechnologies, Faculty of Chemical Technology, University of Pardubice, Nam. Cs. Legii 565, 530 02 Pardubice, Czech Republic. E-mail: jan.macak@upce.cz; Tel: +420466037401

resolution TEM (HRTEM, FEI Titan) equipped with the STEM mode and EDX mapping.

Fig. 1 shows the top-view SEM images of the blank TiO_2-annealed (400 °C) nanotube layers with different average nanotube diameters: (A) 35 nm, (B) 56 nm, and (C) 95 nm. The SEM images D–F represent top-view images of the corresponding TiO_2 nanotube layers coated with CdS *via* ALD. An obvious increase in the wall thicknesses and thus smaller inner nanotube diameters between the blank and coated nanotube layers can be observed, which unequivocally indicates the presence of the CdS coating. To demonstrate that the TiO_2 nanotube layers with different diameters are homogeneously coated with CdS throughout the entire thickness of all layers (approx. 600 nm), cross-sectional SEM analyses of the CdS-coated nanotube layers were carried out. These analyses verified that the nanotubes were indeed well-coated from top to bottom, as well as within the interiors and exteriors in all the nanotube layers. Representative cross-sectional SEM images are shown as insets in Fig. 1.

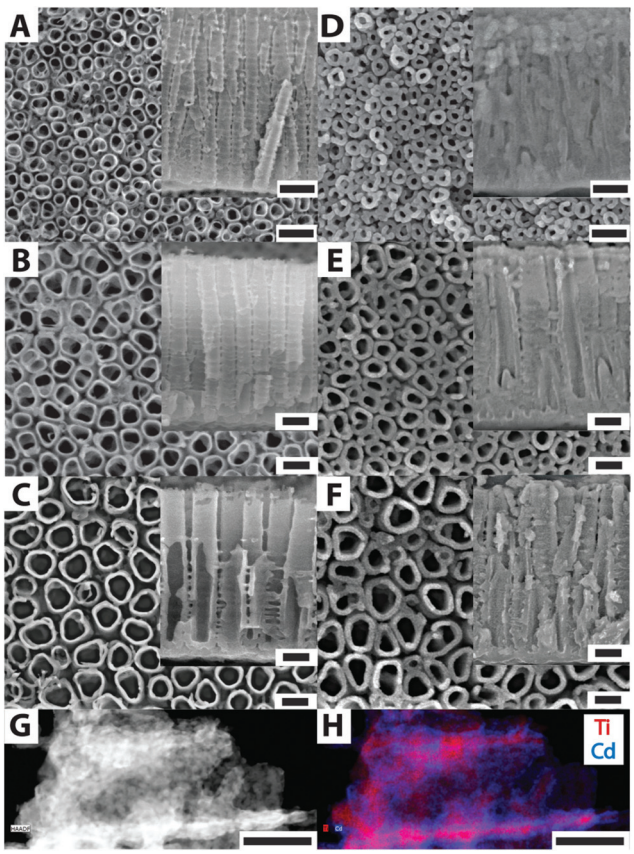

Fig. 1 SEM top-view images of the self-organized TiO_2 nanotube layers with different average nanotube diameters annealed at 400 °C: (A) 35 nm, (B) 56 nm, and (C) 95 nm. SEM images D–F represent the top-view images of the corresponding TiO_2 nanotube layers coated with CdS *via* ALD. Cross-sectional SEM images of the corresponding TiO_2 nanotube layers and CdS-coated counterparts are shown as insets. (G) STEM image of a fragment of CdS-coated TiO_2 nanotube, (H) EDX map of the corresponding STEM image showing Cd and Ti distribution. All scale bars show the distance of 100 nm.

Fig. 1G and H show an STEM image and an EDX map, respectively, of the CdS-coated nanotube shown in Fig. 1F. Evidently, the Cd species (forming CdS) are present throughout the TiO_2 nanotube, in line with the expectation of a uniform ALD coating.[27,28]

It was supposed that the significant increase in the number of nanotubes per cm^2 could have the potential to enhance the photocurrent response of the heterostructured solar cells due to an increase in the interfacial surface area between the chromophore (produced as a conformal coating by ALD) and the TiO_2 nanotube layers. The estimated overall surface areas obtained *via* simple calculations per 1 cm^2 of the TiO_2 nanotube layer for the used TiO_2 nanotube layers are as follows: 52, 29, and 23 cm^2/cm^2 of the macroscopic geometrical area for 35, 56, and 95 nm inner diameters of the TiO_2 nanotubes, respectively.

To obtain information about the photoelectrochemical properties of the nanotube layers and the CdS-coated TiO_2 nanotube layer heterostructures, photocurrent measurements were carried out in an aqueous electrolyte containing 0.1 M Na_2SO_4 *via* employing a photoelectric spectrophotometer (Instytut Fotonowy) in the wavelength range of 300–650 nm at 0.4 V *vs.* Ag/AgCl reference electrode.[21] Apparently, the coupling of CdS coatings with TiO_2 nanotube layers causes a strong sensitizing effect, as shown in Fig. 2. First, the photocurrent density under UV light is enhanced several times as compared to that of the blank TiO_2 nanotube layers. We believe that this phenomenon is related to the annihilation of the surface states during ALD of CdS, which significantly improves the charge collection efficiency, as demonstrated in previous works.[20,21,30,31] More importantly, a robust photocurrent density can be observed in the visible spectral range, peaking at a wavelength of 470 nm. The obtained incident photon-

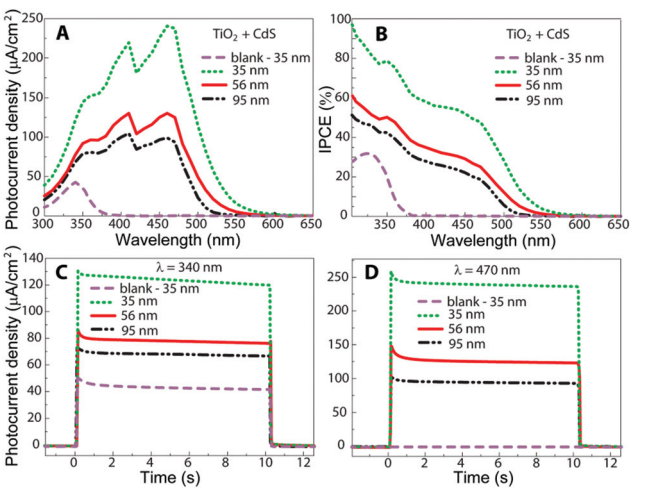

Fig. 2 (A) Photocurrent density and (B) incident photon-to-electron conversion efficiency; (C) and (D) photocurrent transients at 340 nm and 470 nm, respectively, obtained for anatase TiO_2 nanotube layers annealed at 400 °C with different diameters sensitized with crystalline CdS films deposited *via* ALD.

to-electron conversion efficiencies (IPCE), as shown in Fig. 2B, are significantly higher than the previously reported values for chalcogenide-sensitized TiO_2 nanotube layers obtained by chemical bath deposition,[8,19] spincoating,[20,21] and electrodeposition;[22] this is due the fact that the ALD coating of CdS leads to the largest possible interfacial contact area with the TiO_2 nanotube layers obtained from these techniques.

In addition, we found that the obtained photocurrent density increased approximately by a factor of 2 with the downscaling of the TiO_2 nanotube diameter from 95 to 35 nm in the spectral range from 300 to 500 nm. This result perfectly coincides with the increased active surface area of the TiO_2 nanotube layers in the same range of nanotube diameters. Thus, our findings corroborate the assumption that an increase of the interfacial surface area between the chromophore and the TiO_2 nanotube layers should generate higher photocurrent density due to the larger amount of CdS absorber deposited *via* ALD. Conclusively, the combination of 1D nanostructured TiO_2 nanotube layers with a thin light absorber deposited *via* ALD opens a door for a new approach for the fabrication of efficient novel hybrid solar cells. For the energy diagram of the CdS/TiO_2 heterostructure, we refer to previously reported literature.[25,32]

Further, we investigated the influence of thermal treatment of the uncoated TiO_2 nanotube layers on the photoresponse of the subsequently prepared heterostructures based on CdS-coated TiO_2 nanotube layers. For this experiment, we selected nanotube layers with an inner diameter of 35 nm since they have demonstrated the highest IPCE in the entire spectral range (300–650 nm). It can be seen from Fig. 3A and B that photocurrent densities and IPCE of the CdS-coated TiO_2 heterostructures increased with the increasing temperature prior to annealing of the TiO_2 nanotube layers in the temperatures range from 300 to 600 °C.

The enhancement in IPCE is not linear with the increasing temperature and can be divided into 3 steps. The most intensive improvement in IPCE was observed when TiO_2 nanotube layers were pre-annealed from 300 to 400 °C. Next, it seems that annealing of TiO_2 nanotube layers at 400 and 500 °C has a similar effect while annealing at 600 °C, which leads to the anatase to rutile transition,[29] adds further contribution to IPCE.

To obtain a deeper understanding of this phenomenon, we obtained the FE-SEM top-view images of the CdS-coated TiO_2 nanotube layers (see Fig. 3C–F) in combination with the X-ray diffraction patterns (see Fig. 4). At first, it can be seen that the level of the TiO_2 nanotube layer coverage by CdS is noticeably different. While the TiO_2 nanotube layers pre-annealed at 300 °C are decorated with the CdS nanoparticles, as demonstrated in Fig. 3C, a compact and uniform CdS crystalline coating is formed on the TiO_2 nanotube layers pre-annealed at 400, 500, and 600 °C (see Fig. 3D–F). These results indicate that CdS deposition on TiO_2 nanotubes *via* ALD strongly depends on the TiO_2 crystallinity. In the case of TiO_2 nanotube layers pre-annealed at 300 °C, the incubation time for CdS nucleation seems to be longer than that for all other samples pre-annealed at higher temperatures. As a consequence of this,

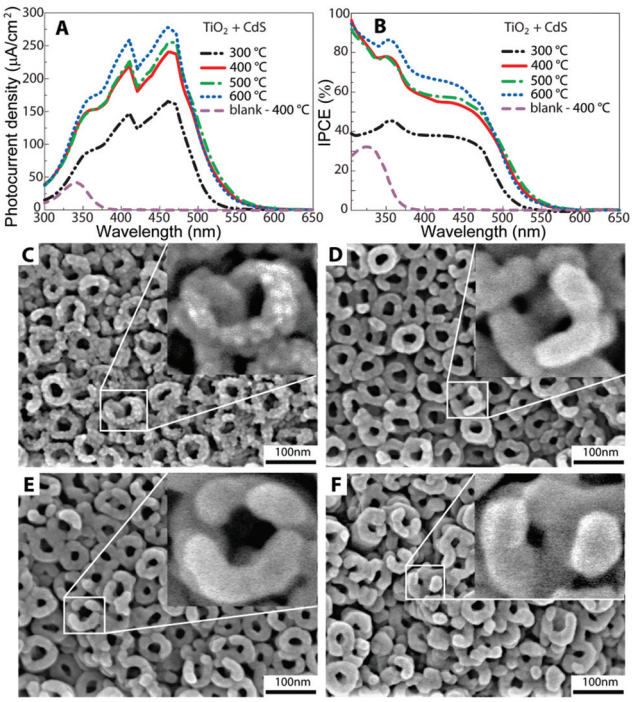

Fig. 3 (A) Photocurrent density and (B) incident photon-to-electron conversion efficiency (IPCE) obtained for the anatase TiO_2 nanotube layers with a 35 nm inner diameter annealed at 300, 400, 500, and 600 °C and sensitized with crystalline CdS films *via* ALD. (C) to (F) represent the top view SEM images of the CdS-coated TiO_2 nanotube layers annealed at (C) 300 °C, (D) 400 °C, (E) 500 °C, and (F) 600 °C.

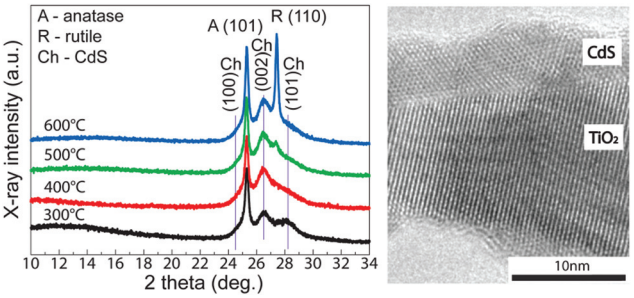

Fig. 4 Bragg diffractions of the TiO_2 nanotube layers with a 35 nm inner diameter annealed at 300, 400, 500, and 600 °C and sensitized with crystalline CdS films deposited by ALD (left panel). The HRTEM image of the TiO_2 nanotube layer pre-annealed at 400 °C and coated with CdS (right panel).

these TiO_2 nanotube layers are only decorated by CdS nanoparticles, leading to lower total mass of CdS and thus lower IPCE. Since it is evident from XRD that the background in the range of 2 theta from 10 to 22° has different shape for this particular TiO_2 nanotube layer pre-annealed at 300 °C, indicating the presence of an amorphous phase, it can be speculated that the CdS nanoparticle growth can be attributed to the incomplete transformation of the originally amorphous TiO_2 nanotubes to the anatase phase. On the other hand, TiO_2 nanotube layers pre-annealed at higher temperatures template the crystal

growth of CdS, which corresponds to the well-evolved crystals. Overall, these findings are well supported by the literature stating that different crystallinity of substrates used for ALD leads to different ALD deposition progress.[33,34]

The templating effect is also obvious from the XRD patterns and the HRTEM image. CdS crystallizes in the hexagonal phase within the space group $P6_3mc$[35] and lattice parameters a = 4.16 Å and c = 6.68 Å. Both the anatase and the rutile modifications possess one cubic face with the lattice parameters a = 3.784 Å (space group $I4_1/amd$)[36] and a = 4.594 Å (space group $P4_2/mnm$),[36] which results in lattice mismatches with CdS 10% and 10.4%, respectively. Since the lattice mismatch between CdS and TiO_2 phases is small, the nucleation and subsequent crystal growth can proceed fast. From the XRD patterns, it can be seen that CdS crystallizes with the preferential orientation along the crystallographic plane (002), which is more pronounced with increasing pre-annealing temperature of the TiO_2 nanotube layers. This observation also supports the idea that fully crystalline TiO_2 nanotube layers, pre-annealed at temperatures at/above 400 °C, are suitable matrices for the ALD deposition of uniform CdS coatings.

Conclusions

We presented photoelectrochemical results for anodic TiO_2 nanotube layers grown with different diameter sizes (35, 56, and 95 nm) with a thickness of approx. 600 nm sensitized with 6 nm thick CdS coatings deposited *via* ALD. We found that the obtained photocurrents increased approximately by a factor of 2 with the downscaling of the TiO_2 nanotube diameter from 95 to 35 nm in the spectral range from 300 to 500 nm. The result perfectly coincides with the increased active surface area of the TiO_2 nanotube layers in the same range of nanotube diameters. We also demonstrated the effect of annealing temperature of TiO_2 nanotube layers on the photocurrent generation of the CdS-coated TiO_2 nanotube layer photochemical cell. This study unequivocally showed that nanotube layers pre-annealed at temperatures higher than 400 °C generated higher photocurrent density in the spectral range from 350 to 550 nm than the nanotube layers pre-annealed at 300 °C due to the presence of an amorphous phase. Finally, we showed the added value of ALD for uniform coating of the nanotube layers by a functional secondary material.

Acknowledgements

European Research Council (project no. 638857) and Ministry of Youth, Education and Sports of the Czech Republic (projects no. LM2015082 and CZ.02.1.01/0.0/0.0/16_013/0001829) are acknowledged for financial support of this work. We thank Dr. Veronika Podzemna, assoc. prof. Ludvik Benes and Dr. Klara Cepe (RCPTM Olomouc) for SEM, XRD and HRTEM analyses, respectively.

Notes and references

1 M. A. Green, K. Emery, Y. Hishikawa, W. Warta and E. D. Dunlop, *Prog. Photovoltaics*, 2016, **24**, 905–913.
2 D. E. Carlson and C. R. Wronski, *Appl. Phys. Lett.*, 1976, **28**, 671.
3 J. Britt and C. Ferekides, *Appl. Phys. Lett.*, 1993, **62**, 2851.
4 P. Jackson, D. Hariskos, E. Lotter, S. Paetel, R. Wuerz, R. Menner, W. Wischmann and M. Powalla, *Prog. Photovoltaics*, 2011, **19**, 894–897.
5 T. K. Todorov, J. Tang, S. Bag, O. Gunawan, T. Gokmen, Y. Zhu and D. B. Mitzi, *Adv. Energy Mater.*, 2013, **3**, 34–38.
6 B. O'Regan and M. Grätzel, *Nature*, 1991, **353**, 737–740.
7 A. Kojima, K. Teshima, Y. Shirai and T. Miyasaka, *J. Am. Chem. Soc.*, 2009, **131**, 6050–6051.
8 W.-T. Sun, Y. Yu, H.-Y. Pan, X.-F. Gao, Q. Chen and L.-M. Peng, *J. Am. Chem. Soc.*, 2008, **130**, 1124–1125.
9 D. Zhao and Ch.-F. Yang, *Renewable Sustainable Energy Rev.*, 2016, **24**, 1048–1059.
10 H. Wang, G. Wang, Y. Ling, M. Lepert, C. Wang, J. Z. Zhang and Y. Li, *Nanoscale*, 2012, **4**, 1463–1466.
11 M. Liu, M. M. Johnston and H. J. Snaith, *Nature*, 2013, **501**, 395–398.
12 J. M. Macak, H. Tsuchiya, A. Ghicov, K. Yasuda, R. Hahn, S. Bauer and P. Schmuki, *Curr. Opin. Solid State Mater. Sci.*, 2007, **11**, 3–18.
13 S. So, I. Hwang and P. Schmuki, *Energy Environ. Sci.*, 2015, **8**, 849–854.
14 W. S. Kim, Y. G. Jang, D. H. Kim, H. C. Kim and S. H. Hong, *CrystEngComm*, 2012, **14**, 4963–4966.
15 Y. J. Hwang, C. Hahn, B. Liu and P. Yang, *ACS Nano*, 2012, **6**, 5060–5069.
16 X. Li, J. Yu, J. Low, Y. Fang, J. Xiao and X. Chen, *J. Mater. Chem. A*, 2015, **3**, 2485–2534.
17 H. Mirabolghasemi, N. Liu, K. Lee and P. Schmuki, *Chem. Commun.*, 2013, **49**, 2067–2069.
18 Z. Miao, D. Xu, J. Ouyang, G. Guo, X. Zhao and Y. Tang, *Nano Lett.*, 2002, **2**, 717–720.
19 X. F. Gao, H. B. Li, W. T. Sun, Q. Chen, F. Q. Tang and L. M. Peng, *J. Phys. Chem. C*, 2009, **113**, 7531–7535.
20 J. M. Macak, T. Kohoutek, L. Wang and R. Beranek, *Nanoscale*, 2013, **5**, 9541–9545.
21 M. Krbal, H. Sopha, V. Podzemna, S. Das, J. Prikryl and J. M. Macak, *J. Phys. Chem. C*, 2017, **121**, 6065–6071.
22 J. A. Fernandes, P. Migowski, Z. Fabrim, A. F. Feil, G. Rosa, S. Khan, G. J. Machado, P. F. P. Fichtner, S. R. Teixeira, M. J. L. Santos and J. Dupont, *Phys. Chem. Chem. Phys.*, 2014, **16**, 9148–9153.
23 S. Das, H. Sopha, M. Krbal, R. Zazpe, V. Podzemna, J. Prikryl and J. M. Macak, *ChemElectroChem*, 2017, **4**, 495–499.
24 S. S. Kalanur, S. H. Lee, Y. J. Hwang and O.-S. Joo, *J. Photochem. Photobiol., A*, 2013, **259**, 1–9.

25 F. Tian, D. Hou, F. Hu, K. Xie, X. Qiao and D. Li, *Appl. Surf. Sci.*, 2017, **391**, 295–302.
26 H. Cai, Q. Yang, Z. Hu, Z. Duan, Q. You, J. Sun, N. Xu and J. Wu, *Appl. Phys. Lett.*, 2014, **104**, 053114.
27 R. Zazpe, M. Knaut, H. Sopha, L. Hromadko, M. Albert, J. Prikryl, V. Gärtnerova, J. W. Bartha and J. M. Macak, *Langmuir*, 2016, **32**, 10551–10558.
28 R. Zazpe, J. Prikryl, V. Gärtnerova, K. Nechvilova, L. Benes, L. Strizik, A. Jäger, M. Bosund, H. Sopha and J. M. Macak, *Langmuir*, 2017, **33**, 3208–3216.
29 S. Das, R. Zazpe, J. Prikryl, P. Knotek, M. Krbal, H. Sopha, V. Podzemna and J. M. Macak, *Electrochim. Acta*, 2016, **213**, 452–459.
30 J. W. Zheng, A. Bhattcahrayya, P. Wu, Z. Chen, J. Highfield, Z. Dong and R. Xu, *J. Phys. Chem. C*, 2010, **114**, 7063–7069.
31 T. Umebayashi, T. Yamaki, H. Itoh and K. Asai, *Appl. Phys. Lett.*, 2002, **81**, 454–456.
32 Y.-L. Lee and Y.-S. Lo, *Adv. Funct. Mater.*, 2009, **19**, 604–609.
33 R. S. Pessoa, F. P. Pereira, G. E. Testoni, W. Chiappim, H. S. Maciel and L. V. Santos, *J. Integr. Circuits Syst.*, 2015, **10**, 38–42.
34 H. B. R. Lee and S. Bent, *Chem. Mater.*, 2012, **24**, 279–286.
35 A. A. Andreev, M. F. Bulanyi, S. A. Golikov and L. A. Mozharovsikii, *Russ. J. Inorg. Chem.*, 1995, **40**, 1039–1042.
36 D. W. Kim, N. Enomoto, Z. Nakagawa and K. Kawamura, *J. Am. Ceram. Soc.*, 1996, **79**, 1095–1099.